Entangled phonons in atomic Bose-Einstein condensates

Stefano Finazzi[1,2,*] and Iacopo Carusotto[2,†]

[1]*Laboratoire Matériaux et Phénomènes Quantiques, Université Paris Diderot-Paris 7 and CNRS, Bâtiment Condorcet, 10 rue Alice Domon et Léonie Duquet, 75205 Paris Cedex 13, France*

[2]*INO-CNR BEC Center and Dipartimento di Fisica, Università di Trento, via Sommarive 14, 38123 Povo–Trento, Italy*

(Received 26 September 2013; revised manuscript received 31 July 2014; published 8 September 2014)

We theoretically propose the measurement of phonon entanglement as a tool to study the quantum dynamics of atomic Bose-Einstein condensates. In particular, we show that nonseparability of the phonon modes offers a unambiguous signature of the quantum origin of the phonon emission by analog Hawking and dynamical Casimir processes. The method is numerically validated by applying a generalized Peres-Horodecki criterion to a truncated Wigner description of the condensate. Viable strategies to implement the proposed scheme in state-of-the-art experiments are discussed.

DOI: 10.1103/PhysRevA.90.033607 PACS number(s): 03.75.Gg, 42.50.Lc, 04.60.−m

I. INTRODUCTION

Pairs of entangled photons are a crucial element of many quantum optical experiments, from Hong-Ou-Mandel two-photon interference [1], to fundamental tests of Bell inequalities [2], to linear optical schemes for quantum information processing [3]. Following the dramatic advances in cooling and manipulating atomic samples, many groups have recently demonstrated entanglement effects using atomic matter waves: Among the most striking observations are nonclassical violations of the Cauchy-Schwartz inequalities in the product of atomic collisions [4,5] and noise reduction in atomic interferometry experiments using squeezed matter fields [6,7].

A most exciting challenge is now to extend quantum optical concepts from single-particle excitations such as photons or atoms to the collective hydrodynamic degrees of freedom of a macroscopic fluid. The experimental investigation of *quantum hydrodynamical* entangled states[1] is in fact a fundamental step in the study of exquisite quantum effects in macroscopic mechanical systems.[2] Beyond standard quantum information applications, the measurement and the manipulation of collective variable entanglement using quantum optical techniques represent promising tools also for the investigation of atomic many-body systems undergoing large quantum fluctuations, e.g., close to a quantum phase transition [11], as already proposed in the context of spin systems [12–16].

Among the first proposals in this *quantum hydrodynamics* direction, the pioneering work [17] anticipated that quantum hydrodynamical fluctuations in a moving fluid are converted at a black-hole sonic horizon into pairs of propagating phonons via a mechanism analogous to the Hawking effect of gravitational physics [18]. Since then, this analogy between phonons in fluids and quantum fields on curved space-times has experienced impressive developments [19]. In particular, atomic Bose-Einstein condensates (BECs) appear as most promising platforms where one can study the conversion of quantum fluctuations into entangled pairs of real phonons: Acoustic Hawking radiation (HR) is expected when an acoustic horizon is present in a stationary flowing BEC [20,21]. On the other hand, a rapid temporal variation of the speed of sound in homogeneous fluids [22–26] leads to the emission of pairs of opposite momentum phonons via a process analogous to the dynamical Casimir effect (DCE) [27,28] and to particle production in an expanding universe [29,30]. Experimental research along these lines is presently very active: The emission of classically correlated pairs was observed in a temporally modulated BEC [31] and a sonic horizon was realized in a flowing BEC [32].

As proposed in Refs. [26,33,34], an important window on these emission phenomena is offered by the correlation function of density fluctuations. However, while this quantity encodes detailed information on the emission geometry and is robust against a nonzero initial temperature, it does not display any specific signature of the quantum origin of the emission from zero-point fluctuations. Several strategies to fill this gap are presently under study. For instance, nonclassical phonon occupation statistics can be revealed by violations of Cauchy-Schwartz inequalities, as proposed in Ref. [35]. A yet stronger signature of the quantum origin of the emission would be the nonseparability of the phonon state. From a purely theoretical point of view this question was addressed in various contexts: time-modulated atomic BECs [36], analog black holes in BECs [37,38] and ion rings [39], fluids of light [40], and generic dissipative media [41,42]. Still, little attention was devoted to experimental strategies to actually detect this entanglement.

In this paper we propose a realistic scheme to experimentally measure the entanglement between the phonon degrees of freedom of an atomic BEC. The theoretical framework and the general principles of the method are presented in Sec. II. In Sec. III, the efficiency of the method is illustrated on the spatial and spectral entanglement pattern of phonons emitted by analog DCE and HR processes in one-dimensional condensates: Specific signatures of the quantum origin of these emissions from zero-point fluctuations are identified. Viable strategies to experimentally implement our proposal in realistic

*stefano.finazzi@univ-paris-diderot.fr

†carusott@science.unitn.it

[1]Note that the term *quantum hydrodynamics* is used here in a somehow stricter sense than in most many-body literature where it broadly refers to generic hydrodynamic effects in a quantum fluid.

[2]See Refs. [8–10] for examples of entanglement in macroscopic optical systems.

setups are discussed in Sec. IV. Conclusions are finally drawn in Sec.V.

II. THEORETICAL FRAMEWORK

A. Generalized Peres-Horodecki (GPH) criterion

Among the many available criteria to assess whether the state of a bipartite system is entangled [43], we adopt the one proposed by Peres and Horodecki [44,45] and later extended in Refs. [46,47] to the continuous variable case of present interest. Consider two generic degrees of freedom $j = 1,2$ described by the pairwise canonically conjugated operators $\hat{q}_j$ and $\hat{p}_j$. We group these operators in a vector $\hat{X} \equiv (\hat{q}_1, \hat{p}_1, \hat{q}_2, \hat{p}_2)$, with expectation value $\bar{X} = \langle \hat{X} \rangle_{\hat{\rho}} = \mathrm{tr}(\hat{X}\hat{\rho})$ and covariance matrix $V_{\alpha\beta} = \frac{1}{2}\langle \Delta\hat{X}_\alpha \Delta\hat{X}_\beta + \Delta\hat{X}_\beta \Delta\hat{X}_\alpha \rangle_{\hat{\rho}}$, where $\Delta\hat{X} = \hat{X} - \langle \hat{X} \rangle$.

Following Ref. [47], the generalized Perez-Horodecki (GPH) criterion states that if a state is separable, then the GPH function $\mathcal{P}$ defined as

$$\mathcal{P} \equiv \det A \det B + \left(\frac{1}{4} - |\det C|\right)^2 - \mathrm{tr}[AJCJBJC^T J] - \frac{1}{4}(\det A + \det B) \quad (1)$$

is positive. Here A, B, C are 2×2 submatrices of V and J is the 2×2 simplectic matrix,

$$V = \begin{pmatrix} A & C \\ C^T & B \end{pmatrix}, \quad J = \begin{pmatrix} 0 & 1 \\ -1 & 0 \end{pmatrix}. \quad (2)$$

B. Phonon operators

To practically use the GPH criterion to assess phonon entanglement in a specific configuration, one must first identify the relevant degrees of freedom and construct the corresponding $\hat{q}_j$ and $\hat{p}_j$ operators in terms of the microscopic phonon operators. The associated bosonic operators then read $\hat{a}_j = (\hat{q}_j + i\,\hat{p}_j)/\sqrt{2}$ and satisfy bosonic commutation rules $[\hat{a}_j, \hat{a}_l] = 0$ and $[\hat{a}_j, \hat{a}_l^\dagger] = \delta_{jl}$.

To capture phonon entanglement features in both real and momentum spaces, it is convenient to introduce phonon wave-packet operators $\hat{a}_{k,x_0}$ defined by projecting the full atomic field $\hat{\Psi}(x)$ onto a localized phonon wave packet,

$$\hat{a}_{k,x_0} = \int dx\, f^*_{k,x_0}(x)[u_k\, \hat{\Phi}(x) - v_k \hat{\Phi}(x)^\dagger], \quad (3)$$

with the Gaussian envelope

$$f_{k,x_0}(x) = (\pi\sigma^2)^{-1/4} e^{-(x-x_0)^2/2\sigma^2} e^{ik(x-x_0)} \quad (4)$$

centered at a spatial position x_0, of width σ and carrier wave vector k. Generalization of this one-dimensional formula to two- and three-dimensional cases is straightforward. The exponential factor in the definition $\hat{\Phi}(x) \equiv e^{-i(Kx-\Omega t)}\,\hat{\Psi}(x)$ takes into account the space and time dependence of the condensate phase with wave vector K and frequency $\Omega = \hbar K^2/2m + gn$. The Bogoliubov coefficients u_k and v_k serve to extract the phonon amplitude from the full atomic field. As usual [48], they are defined by

$$u_k \pm v_k = \left(\frac{\varepsilon_k}{\varepsilon_k + 2\mu}\right)^{\pm 1/4} \quad (5)$$

in terms of the kinetic and interaction energies $\varepsilon_k = \hbar^2 k^2/2m$ and $\mu = gn$, where m is the atomic mass, n the one-dimensional density, and g the effective one-dimensional interaction constant [34].

The phonon entanglement involves the measurement of phonon operators $\hat{a}_1 = \hat{a}_{k_1,x_1}$ and $\hat{a}_2 = \hat{a}_{k_2,x_2}$ centered at different wave vectors $k_{1,2}$ and different spatial positions $x_{1,2}$. As a first step, one must ensure that these $\hat{a}_{1,2}$ indeed satisfy the proper bosonic commutation rules. Using the canonical commutation relation for $\hat{\Psi}$ and assuming $\sigma|k_{1,2}| \gg 1$ to suppress overlap with the condensate mode [48], one can write the commutators as

$$[\hat{a}_{k_1,x_1}, \hat{a}_{k_2,x_2}] = (v_{k_1}u_{k_2} - u_{k_1}v_{k_2}) e^{i(x_1-x_2)(k_1-k_2)/2} \times e^{-(x_1-x_2)^2/4\sigma^2} e^{-\sigma^2(k_1+k_2)^2/4}, \quad (6)$$

$$[\hat{a}_{k_1,x_1}, \hat{a}^\dagger_{k_2,x_2}] = (u_{k_1}u_{k_2} - v_{k_1}v_{k_2}) e^{i(x_1-x_2)(k_1+k_2)/2} \times e^{-(x_1-x_2)^2/4\sigma^2} e^{-\sigma^2(k_1-k_2)^2/4}. \quad (7)$$

As expected, all commutators vanish when the two points $x_{1,2}$ are separated by a distance $|x_1 - x_2| \gg \sigma$. Under the assumed condition $\sigma|k_{1,2}| \gg 1$, one has $[\hat{a}_{k_1,x_1}, \hat{a}_{k_2,x_2}] \approx 0$ for any value of $|x_1 - x_2|$. Furthermore, $[\hat{a}_{k_1,x_1}, \hat{a}^\dagger_{k_2,x_2}] \approx 0$ for well-separated momenta $\sigma|k_1 - k_2| \gg 1$, while it tends to 1 for wave packets overlapping in both real ($|x_1 - x_2| \ll \sigma$) and momentum ($\sigma|k_1 - k_2| \ll 1$) spaces.

Summarizing, a sufficient condition for the $\hat{a}_1 = \hat{a}_{k_1,x_1}$ and $\hat{a}_2 = \hat{a}_{k_2,x_2}$ phonon operators to satisfy the desired bosonic commutation rules is that the positions are well separated in space $|x_1 - x_2| \gg \sigma$ and the wave vectors are well separated from each other $\sigma|k_1 - k_2| \ll 1$ and from zero $\sigma|k_{1,2}| \gg 1$.

C. Calculation of the GPH function

An efficient tool to calculate the covariance matrix V and the GPH function $\mathcal{P}$ in a realistic configuration is provided by the truncated Wigner method [49,50]: The quantum field is represented in terms of a stochastic classical field distributed according to the so-called Wigner distribution and the expectation value of any symmetrized operator is obtained as the average of the corresponding classical quantity.

In our calculations, we numerically sampled the Wigner distribution [34] using a large number N_r of stochastic wave functions $\Psi^{j=1,\ldots,N_r}(x,t)$: The initial conditions $\Psi^j(x, t=0)$ are chosen in a way to reproduce either the ground state or a thermal distribution at the desired T. At later times $t > 0$, each realization $\Psi^j(x,t)$ evolves according to a Gross-Pitaevskii equation. At each time, the expectation value of the phonon operators $\hat{a}_{k,x_0}$ are obtained as the average

$$\langle \hat{a}_{k,x_0} \rangle = \frac{1}{N_r} \sum_{j=1}^{N_r} \alpha^j_{k,x_0} \quad (8)$$

of the corresponding classical quantities extracted from each realization $\Psi^j(x,t)$ via the classical counterpart of Eq. (3),

$$\alpha^j_{k,x_0}(t) = \int dx\, f^*_{k,x_0}(x)[u_k \Psi^j(x,t) - v_k \Psi^j(x,t)^*]. \quad (9)$$

Analogously, the elements of the correlation matrix V involved in the GPH function $\mathcal{P}$ via Eq. (1) are obtained as the average of the products of the corresponding classical amplitudes (9).

III. REAL- AND MOMENTUM-SPACE STRUCTURE OF ENTANGLEMENT

A. Analog dynamical Casimir emission

As a first application of our method, in this section we study the entanglement between phonons spontaneously created in spatially homogeneous one-dimensional condensates at rest by a sudden variation of the speed of sound c from c_- at $t = 0^-$ to c_+ at $t = 0^+$, obtained, e.g., via a modulation of the atomic interaction constant. This quench process is a condensed-matter analog of the DCE and of the spontaneous particle creation in an expanding universe [22,23,25,26,51]. While the classical correlations experimentally observed in Ref. [31] originate from thermally stimulated processes, detection of entanglement in the same experiment starting from a lower initial temperature would be an unambiguous signature of quantum processes. A first theoretical study in this direction [36] was restricted to correlations in wave-vector space. Here we extend the discussion by unveiling peculiar structures in the space-wave-vector entanglement pattern.

In Fig. 1 we display the region in the k_1-k_2 momentum plane where the GPH function $\mathcal{P}$ is negative. The numerical observation is performed at the same time $t = t_{\rm obs} = 120\hbar/\mu_-$, for different distances, $\Delta x = x_2 - x_1 = 120\xi_-$ (left panels) and $240\xi_-$ (right), and initial temperatures $k_B T/\mu_- = 0$ (top) and 0.2 (bottom), measured in units of the initial $\mu_- = mc_-^2$ and healing length $\xi_- = \hbar/mc_-$. According to translational invariance, entanglement is visible only between phonons with opposite wave vectors $k_1 = -k_2$ (up to an uncertainty $1/\sigma$ set by the wave-packet size). In analogy with density correlations [26,52], entanglement for a vanishing initial temperature $T = 0$ (upper panels) is strongest at $|k_{1,2}| = \bar{k} = 0$ (left) and $0.93/\xi_-$ (right), satisfying the ballistic condition $2v^{\rm gr}(\bar{k})t_{\rm obs} = \Delta x$, where $v^{\rm gr}(k) = d\omega/dk$ is the group velocity derived by the Bogoliubov dispersion $\omega^2 = c^2k^2 + \hbar^2k^4/4m^2$.

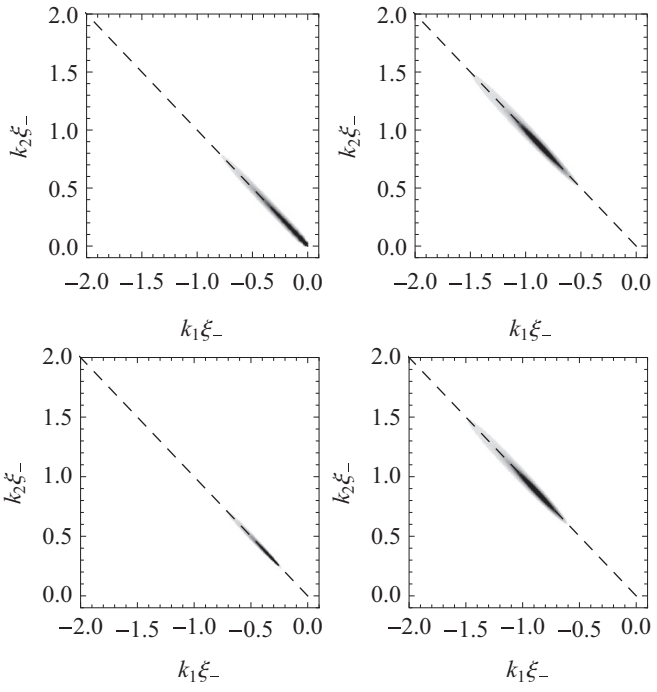

FIG. 1. Entanglement between phonons generated by the analog DCE. The shading indicates the regions of the k_1-k_2 momentum plane where the GPH function $\mathcal{P} < 0$ (darker gray, larger $|\mathcal{P}|$) for wave packets centered at $\Delta x = |x_1 - x_2| = 120\xi_-$ (left) and $240\xi_-$ (right) with $\sigma = 35\xi_-$, at $k_B T/\mu_- = 0$ (top) and 0.2 (bottom). Dashed lines indicate $k_2 = -k_1$. In all plots $t_{\rm obs} = 120\hbar/\mu_-$.

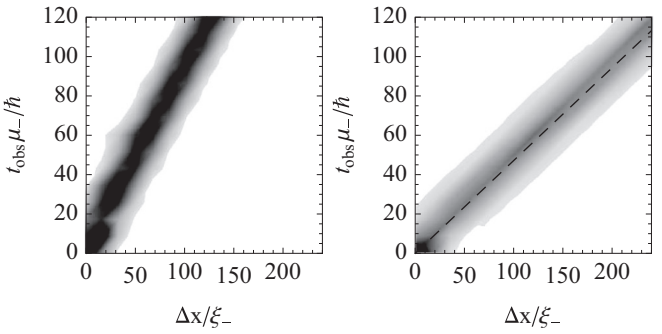

FIG. 2. Entanglement between phonons generated by the analog DCE. The shading indicates the region of the Δx-$t_{\rm obs}$ plane where the GPH function $\mathcal{P} < 0$ (darker gray, larger $|\mathcal{P}|$) for wave packets with $k_2 = -k_1 = 0.25/\xi_-$ (top) and $1/\xi_-$ (bottom) with $\sigma = 15\xi_-$, at $T = 0$. Dashed lines indicate $t_{\rm obs} = \Delta x/2|v^{\rm gr}(k_{1,2})|$. In all plots $t_{\rm obs} = 120\hbar/\mu_-$.

However, in contrast to density correlations, which are reinforced by thermally stimulated processes, entanglement is very sensitive to the zero-point nature of the initial fluctuations. The decrease of the signal for growing temperatures is apparent when comparing the upper and lower panels. In agreement with Ref. [36], entanglement disappears first at low k (lower left), because of the large initial thermal occupation of low-k modes, while it is more robust at large k (lower right). Overall, entanglement persists up to $k_B T/\mu_- \simeq 0.615$. Note that effective temperatures $k_B T_{\rm eff}/\mu \simeq 1/2$ below this limit were experimentally demonstrated for the asymmetric modes of split one-dimensional condensates in Refs. [53,54]. Arbitrarily lower temperatures are expected for slower, quasiadiabatic splitting sequences.[3]

The peculiar spatial structure of the entanglement pattern is illustrated in Fig. 2, where the GPH function $\mathcal{P}$ is plotted in the Δx-$t_{\rm obs}$ plane for two values $|k_{1,2}| = \tilde{k}$ at $T = 0$. Entanglement is concentrated within a distance σ from the (dashed) straight

[3]This procedure is valid only for one-dimensional systems where symmetric and antisymmetric modes are efficiently decoupled. The initially negligible occupation of the gapped antisymmetric mode remains negligible during the adiabatic splitting. As the HR and DCE occur independently in the symmetric and antisymmetric channels, one only needs a detection scheme that is able to isolate the antisymmetric component of the fluctuations [53,54].

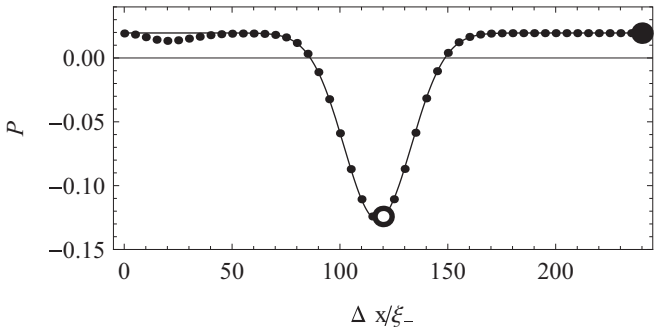

FIG. 3. Cut of the left panel of Fig. 2 along the horizontal dotted line: The GPH $\mathcal{P}$ function is plotted as a function of the distance Δx between the centers of two wave packets with opposite wave vectors $k_2 = -k_1 = 0.25/\xi_-$ and spatial width $\sigma = 15\xi_-$, at $t_{\rm obs} = 110\,\hbar/\mu_-$ after the sudden temporal modulation originating the analog DCE. Solid curve: Best fit of the Gaussian function of Eq. (10); values of the parameters in Eq. (11).

line $t_{\rm obs} = \Delta x/2|v^{\rm gr}(k)|$ whose slope is determined by the selected phonon wave vector $k = \tilde{k}$.

To provide more quantitative insight on the behavior of the GPH function $\mathcal{P}$, in Fig. 3 we plot the numerical values of $\mathcal{P}$ (dots) as a function of Δx for a cut at constant time $t_{\rm obs} = 110\hbar/\mu_-$ of the left panel of Fig. 2, as indicated by the horizontal dotted line. The solid curve is a Gaussian fit of the form

$$f(\Delta x) = \alpha + \beta\, e^{-(\Delta x-\zeta)^2/2\delta^2}, \tag{10}$$

whose parameters α, β, δ, and ζ have been determined through a standard nonlinear chi-squared fit procedure, yielding

$$\alpha \approx 0.0196, \quad \beta \approx -0.146, \quad \delta \approx 15.6\xi_-, \quad \zeta \approx 117\,\xi_-. \tag{11}$$

The presence of entanglement is attested by the negative value of the GPH function $\mathcal{P}$ at the bottom of the dip centered around $\Delta x = \zeta \approx 117\xi_-$. The position of the dip is in good agreement with the separation $\Delta x(t_{\rm obs}) = 2|v^{\rm gr}(\tilde{k})|t_{\rm obs} \approx 120\xi_-$ that is expected for the ballistic propagation of phonons at $\tilde{k} = 0.25/\xi_-$. Moreover, the width $\Delta \approx 15.6\,\xi_-$ of the negative dip well matches the spatial width of the wave packets, $\sigma = 15\,\xi_-$.

To quantify the numerical precision with which the quadrature variances need to be measured to reliably assess entanglement, we quote here the values of the full covariance matrix at the two points indicated in the figure as open and solid dots. The first point is located at the distance value $\Delta x = 120\xi_-$ where entanglement is strongest: Here, the covariance matrix is

$$V_{120} \simeq \begin{pmatrix} 0.624 & 0 & 0.210 & -0.284 \\ 0 & 0.624 & -0.284 & -0.210 \\ 0.210 & -0.284 & 0.624 & 0 \\ -0.284 & -0.210 & 0 & 0.624 \end{pmatrix}. \tag{12}$$

The second point is located at a larger distance $\Delta x = 240\xi_-$ for which the phonon wave-packet operators are effectively uncorrelated. As a result, not only is the submatrix C of the covariance matrix defined in Eq. (2) zero, but the full covariance matrix is diagonal:

$$V_{240} \simeq 0.624\ \mathbf{I}_{4\times4}, \tag{13}$$

where $\mathbf{I}_{4\times4}$ is the 4×4 identity matrix. The numerical values are given with three significant digits and all matrix elements smaller than 10^{-5} have been set to zero.

B. Analog Hawking radiation

As a second application, we characterize the phonon entanglement pattern that results from analog Hawking emission in a flowing condensate displaying a sonic black-hole (BH) horizon. For the sake of simplicity, we focus on the configuration of Ref. [34]: a condensate with homogeneous density $n(x) = n_0$ flowing with a uniform rightward velocity $v(x) = v_0 > 0$ (upper panel of Fig. 4). The sonic horizon is created by a suitable space dependence of both the interaction constant $g(x)$ and the external potential $V(x)$. In the upstream (downstream) region, corresponding to the exterior (interior) of the BH, the flow is subsonic (supersonic) $c(x < 0) = c_{\rm sub} > v_0$ $[c(x > 0) = c_{\rm sup} < v_0]$, while the point $x = 0$, where $c(x) = v_0$, behaves as the sonic horizon. As in Ref. [34], all simulations start from a uniform flow configuration at given T and the horizon is switched on at $t = 0$.

The physical origin of HR can be understood from the Bogoliubov dispersion relation $(\omega - v_0 k)^2 = c^2k^2 + \hbar^2k^4/4m^2$ in the laboratory frame [55,56], shown in the lower panels of Fig. 4 for the subsonic (left) and supersonic (right) regions. Owing to the presence of negative energy modes in the supersonic region, pairs of phonons can be spontaneously created at no energy cost: The emission of a positive energy phonon propagating away from the BH (solid dot) is compensated by the simultaneous emission of a negative energy phonon falling inside the BH (open dot); energy conservation only imposes a relation $\omega_{\rm sub}(k_1) = -\omega_{\rm sup}(k_2)$ between the momenta $k_{1,2}$ of the two emitted phonons.

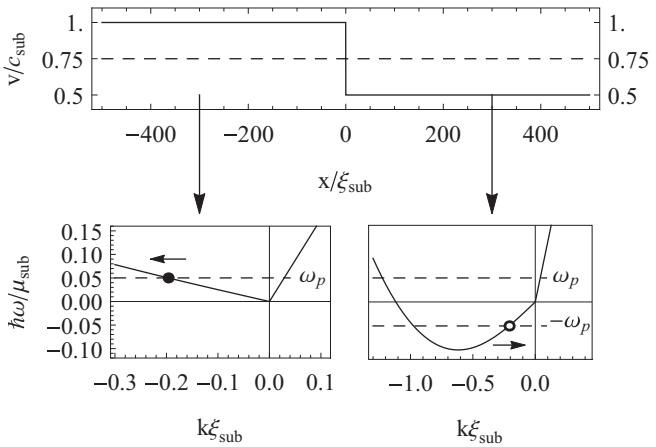

FIG. 4. Flowing condensate showing a sonic horizon at $x = 0$. Upper panel: Flow velocity (dashed line) and speed of sound (solid line). Lower panels: Bogoliubov dispersion in the subsonic (left) and supersonic (right) regions. Open and solid dots indicate the modes where the dominant Hawking emission occurs.

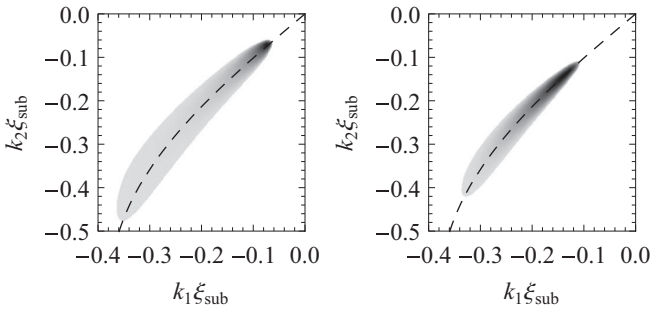

FIG. 5. Entanglement between Hawking phonons. The shading indicates the region of the k_1-k_2 momentum plane where the GPH function $\mathcal{P} < 0$ (darker gray, larger $|\mathcal{P}|$) for initial temperatures $k_B T/\mu_{\rm sub} = 0$ (left) and 0.1 (right) and a late observation time $t_{\rm obs} = 480\hbar/\mu_{\rm sub}$, where $\mu_{\rm sub} = mc^2_{\rm sub}$ in the subsonic region. To optimize the signal the wave packets are located at $x_1 = -61\xi_{\rm sub}$ and $x_2 = 59\xi_{\rm sub}$ with $\sigma = 35\xi_{\rm sub}$. Dashed lines indicate the energy conservation condition (see text). The velocity profile is the one shown in Fig. 4.

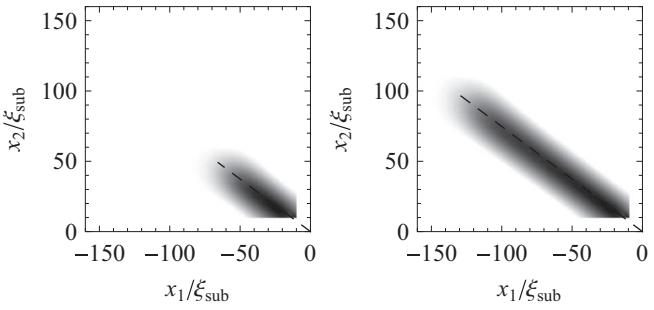

FIG. 6. Entanglement between Hawking phonons. The shading indicates the region of the x_1-x_2 plane where the GPH function $\mathcal{P} < 0$ (darker gray, larger $|\mathcal{P}|$) for different evolution times $t_{\rm obs}\mu_{\rm sub}/\hbar =$ 240 (left) and 480 (right). Wave packets are centered at $k_2 = k_1 = -0.25/\xi_{\rm sub}$ with $\sigma = 15\xi_{\rm sub}$. Initial temperature $T = 0$. Dashed lines indicate the ballistic condition (see text). The velocity profile is the one shown in Fig. 4.

This feature is illustrated in Fig. 5 where the GPH function $\mathcal{P}$ is plotted in the k_1-k_2 plane for two values of the initial temperature $k_B T/\mu_{\rm sub} = 0$ (left) and 0.1 (right) for a late time at which $\mathcal{P}$ has attained its steady-state value; the positions $x_{1,2}$ lie on the two sides of the horizon, respectively. As expected, entanglement is present for pairs of phonons whose wave vectors $k_{1,2}$ are within a distance $1/\sigma$ from the dashed line, indicating the energy conservation condition. This result is the entanglement counterpart of the momentum-space correlations of Ref. [57] and of the sub-Poissonian features of Ref. [35]. As in the DCE case, the entanglement signal first disappears at low k for growing temperatures[4] and eventually completely disappears for $k_B T/\mu_{\rm sub} \gtrsim 0.195$. As already mentioned, temperatures below this bound may be achieved through an adiabatic generalization of the splitting technique of Refs. [53,54].

Finally, the spatial structure of the entanglement pattern in the x_1-x_2 plane is shown in Fig. 6. Wave vectors $k_1 = k_2 = -0.25/\xi_{\rm sub}$ approximately satisfying the energy conservation condition are chosen. Analogously to density correlations [33,34], entanglement is maximum in the vicinity of the dashed lines indicating the ballistic condition $x_1/v^{\rm gr}_{\rm sub}(k_1) = x_2/v^{\rm gr}_{\rm sup}(k_2)$. As Hawking phonons start being emitted after the horizon formation time $t = 0$, entanglement is restricted to the $x_1 > v^{\rm gr}_{\rm sub}(k_1)t_{\rm obs}$ and $x_2 < v^{gr}_{\rm sup}(k_2)t_{\rm obs}$ regions [see the different lengths of the entanglement tongues at $t_{\rm obs}\mu_{\rm sub}/\hbar =$ 240 (left) and 480 (right)].

IV. EXPERIMENTAL REMARKS

In the previous sections we have theoretically studied the entanglement pattern that results from the quantum emission of phonons via DCE and HR processes. Our study was based on numerical data for the covariance matrix V obtained from a truncated Wigner sampling of the atomic quantum field. A practical implementation of our proposal requires a method to efficiently measure the covariance matrix V in an actual experiment: A brief discussion of some possible experimental strategies to perform this task is the subject of this last section. It is interesting to note that a closely related strategy was recently adopted in a quantum optical framework to assess the quantum properties of the DCE emission in a circuit quantum electrodynamics device [58,59].

One possibility to measure the phonon field consists of mapping it onto a bare atomic field through phonon evaporation [31,60] and then performing a homodyne detection of the noncondensed atoms [61–63]. Unfortunately, this technique is likely to require a very precise control of the relative phase of the condensate and the matter-wave local oscillators.

Another, possibly easier, alternative consists of measuring the Fourier component of the atomic density fluctuations corresponding to the phonon mode of interest. For the sake of concreteness, we shall focus our attention on a scheme based on coupling the atomic condensate to an optical cavity which has already been experimentally exploited in a slightly different context. As it was studied in Refs. [64–66], the frequency shift of the optical mode of a cavity enclosing the condensate is proportional to the amplitude of the phonon mode maximizing the overlap with the optical cavity mode. All quadratures of the phonon amplitude can then be reconstructed from a few measurements of the optical mode shift performed at slightly different positions and times, so the complete covariance matrix V is finally obtained by averaging over many realizations of the experiment. While doing so, it is essential to note that some of the matrix elements of V involve noncommuting observables, so clever schemes are needed to reformulate them in terms of commuting observables to be measured on the same realization of the experiment.

[4] A calculation with a smaller σ (not shown) confirms that the weak Hawking emission rate at high k is blurred by the finite-momentum resolution $1/\sigma$: The entanglement band in the k_1-k_2 plane becomes proportionally wider and the entanglement of high-momentum modes disappears at lower temperatures.

A. Phonons and density fluctuations

We begin our discussion from the simplest case of a homogeneous and stationarily flowing one-dimensional Bose-condensed atomic gas. Within the Bogoliubov picture [48,67], we decompose the atomic field into a classical coherent condensate and quantized phonon excitations on top of the condensate,

$$\hat{\Psi}(x) = e^{iKx}\left[\Phi_0 + \int \frac{dk}{2\pi}\left(\hat{a}_k u_k e^{ikx} + \hat{a}_k^\dagger v_k^* e^{-ikx}\right)\right], \quad (14)$$

where K and Ω are the momentum and the frequency of the condensate defined after Eq. (4), Φ_0 is chosen as real and positive, u_k and v_k as real [see Eq. (5)], and $\hat{a}_k$ are bosonic operators describing the amplitude of the plane-wave phonon modes.

Reminding the Bogoliubov form of the atomic density operator,

$$\begin{aligned}\hat{n}(x) &= \hat{\Psi}^\dagger(x)\hat{\Psi}(x) \\ &\approx \Phi_0^2 + \Phi_0 \int \frac{dk}{2\pi}(u_k + v_k)(\hat{a}_k\, e^{ikx} + \text{H.c.}),\end{aligned} \quad (15)$$

it is straightforward to express the $k_0 \neq 0$ component of the Fourier transform of the density in terms of some quadrature of the phonon operators,

$$\hat{n}(k_0) = \int dx\, e^{-ik_0 x}\, \hat{n}(x) = \Phi_0\,(u_k + v_k)\left(\hat{a}_{k_0} + \hat{a}_{-k_0}^\dagger\right). \quad (16)$$

Taking into account the harmonic evolution of free phonon operators at frequency ω_{k_0}, the other quadratures can be extracted by repeating the density measurement at time $\Delta t = \pi/(2\omega_{k_0})$ later, which gives

$$\begin{aligned}\hat{n}(k_0, \Delta t) &= \int dx\, e^{-ik_0 x}\, \hat{n}(x) \\ &= -i\,\Phi_0\,(u_k + v_k)\left(\hat{a}_{k_0} - \hat{a}_{-k_0}^\dagger\right).\end{aligned} \quad (17)$$

A naive look at these formulas might suggest that a complete information on the covariance matrix V could be extracted from a simultaneous measurement of the four observables, $\hat{n}(k_0) \pm \hat{n}^\dagger(k_0)$ and $\hat{n}(k_0, \Delta t) \pm \hat{n}^\dagger(k_0, \Delta t)$, followed by a suitable averaging over realizations. Still, great care has to be paid to the fact that only commuting observables can be simultaneously measured in quantum mechanics and, more generally, measurement of one observable can affect later measurement of other ones.

B. Optomechanical detection of phonons

To firmly assess these issues, from now on we focus our attention on the cavity scheme experimentally pioneered in Refs. [64,65] and sketched in Fig. 7. In such systems, the optomechanical coupling between the cavity mode and the density fluctuations in the atomic condensate can be written in the form [66]

$$\hat{\mathcal{H}}_{\text{int}} = \frac{\mathcal{G}^2}{\Delta}\int dx\, \hat{\mathcal{E}}^\dagger(x)\hat{\mathcal{E}}(x)\hat{n}(x), \quad (18)$$

where $\hat{\mathcal{E}}(x) = \mathcal{E}_c(x)(\hat{c} + \hat{c}^\dagger)$ is the electric field operator in the (single-mode) cavity mode at position x, $\mathcal{G}$ is the atom-light coupling, and Δ is the detuning between the atomic transition

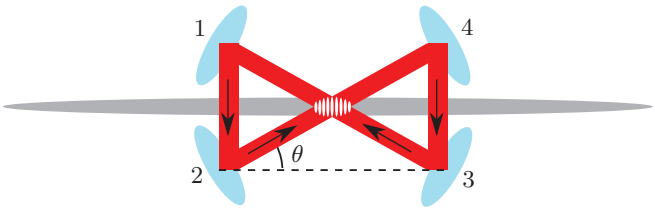

FIG. 7. (Color online) Sketch of the proposed experimental cavity configuration. The cavity mode has a ring structure with two intersecting running waves generating a longitudinal standing-wave pattern in the region of interest.

and the cavity mode frequency. As a most promising example, in the figure we show the eight-shaped running optical mode of a ring cavity enclosed by four mirrors. At the condensate position, the cavity mode consists of a standing wave created by the interference of two intersecting beams forming an angle θ with the condensate velocity. Taking into account the waist σ_c of the cavity mode, the longitudinal profile of the cavity mode in this region has the form

$$\mathcal{E}_c(x) = A\cos\left(\frac{k_0 x}{2}\right)e^{-(x-x_0)^2/2\sigma^2}, \quad (19)$$

where $k_0 = 2k_c\cos\theta$, k_c is the wave vector of the field forming the standing wave in the cavity, and $\sigma = \sigma_c/\sin\theta$ is the spatial size of the measurement region centered at x_0.

Postponing the more realistic case of a finite cavity mode to the next section, we first consider the $\sigma \to \infty$ limit in which the light field in the cavity forms an infinite standing wave. In this limit, the interaction Hamiltonian involves the overlap

$$\begin{aligned}\hat{O}_{k_0} &= 2\int dx\, \hat{n}(x)\cos^2\left(\frac{k_0 x}{2}\right) \\ &= \int dx\, \hat{n}(x)[1 + \cos(k_0 x)] = \Phi_0^2 V + \hat{v}_{k_0},\end{aligned} \quad (20)$$

where the first constant $\Phi_0^2 V$ is the total number of condensate atoms in the interaction region and the fluctuation term $\hat{v}_{k_0}$ involves a combination of phonon operators at $\pm k_0$ of the form

$$\begin{aligned}\hat{v}_{k_0} &= \frac{(u_{k_0} + v_{k_0})\Phi_0}{2}\left(\hat{a}_{k_0} + \hat{a}_{k_0}^\dagger + \hat{a}_{-k_0} + \hat{a}_{-k_0}^\dagger\right) \\ &= \frac{(u_{k_0} + v_{k_0})\Phi_0}{\sqrt{2}}\left(\hat{q}_{k_0} + \hat{q}_{-k_0}\right).\end{aligned} \quad (21)$$

Here, we have used $u_{k_0} = u_{-k_0}$ and $v_{k_0} = v_{-k_0}$ and we have defined the phonon quadrature operators as $\hat{q}_{k_0} = (\hat{a}_{k_0} + \hat{a}_{k_0}^\dagger)/\sqrt{2}$ and $\hat{p}_{k_0} = (\hat{a}_{k_0} - \hat{a}_{k_0}^\dagger)/\sqrt{2}i$.

Noting that the interaction Hamiltonian (18) is of the generic form

$$\hat{\mathcal{H}}_{\text{int}} = G\,\hat{c}^\dagger\,\hat{c}\,\hat{O}_{k_0} \quad (22)$$

in terms of the cavity mode operator $\hat{c}$, a nondestructive measurement of the overlap operator $\hat{O}_{k_0}$ can be obtained by measuring the cavity frequency shift, which in turn can be extracted from the transmission spectrum through the cavity.

In the states of the fluid considered in this work, the expectation value of $\hat{v}_{k_0}$ vanishes $\langle \hat{v}_{k_0} \rangle = 0$, so for each realization of the experiment,

$$\hat{v}_{k_0} = \hat{O}_{k_0} - \langle \hat{O}_{k_0} \rangle = \hat{O}_{k_0} - \Phi_0^2 V. \tag{23}$$

By performing a similar measurement of $\hat{O}_{k_0}$ after a time delay Δt, using a detector spatially displaced by Δx, different combinations of the operators $\hat{a}_{k_0}$, $\hat{a}_{k_0}^\dagger$, $\hat{a}_{-k_0}$, and $\hat{a}_{-k_0}^\dagger$ can be measured:

$$\begin{aligned}\hat{v}_{k_0}(\Delta t, \Delta x) &\equiv \int dx\, n(\Delta t, x) \cos[k_0(x - \Delta x)] \\ &= \frac{(u_{k_0} + v_{k_0})\Phi_0}{2} \big[\hat{a}_{k_0} e^{-i(\omega_{k_0}\Delta t - k_0 \Delta x)} \\ &\quad + \hat{a}_{-k_0} e^{-i(\omega_{-k_0}\Delta t + k_0 \Delta x)} + \text{H.c.}\big],\end{aligned} \tag{24}$$

where

$$\omega_{k_0} = \tilde{\omega}_{k_0} + v k_0, \quad \omega_{-k_0} = \tilde{\omega}_{k_0} - v k_0, \tag{25}$$

$\tilde{\omega}_{k_0}$ is the phonon frequency in the reference frame where the condensate is at rest, and $v = \hbar K/m$ is the velocity of the condensate. Defining the temporal $\Delta\tau$ and comoving spatial $\Delta\chi$ phase shift as

$$\Delta\tau \equiv \tilde{\omega}_{k_0} \Delta t, \quad \Delta\chi \equiv k_0 \Delta x - v \Delta t, \tag{26}$$

all quadratures of interest are grouped in the normalized operators

$$\hat{N}_{k_0}(\Delta\tau, \Delta\chi) \equiv \frac{\sqrt{2}}{\Phi_0 (u_{k_0} + v_{k_0})} \hat{v}_{k_0}(\Delta t, \Delta\tilde{x}), \tag{27}$$

taken at suitable values of $\Delta\tau$ and $\Delta\chi$, namely,

$$\hat{q}_{k_0} + \hat{q}_{-k_0} = \hat{N}_{k_0}(0,0), \tag{28}$$

$$\hat{q}_{k_0} - \hat{q}_{-k_0} = \hat{N}_{k_0}\left(\frac{\pi}{2}, \frac{\pi}{2}\right), \tag{29}$$

$$\hat{p}_{k_0} + \hat{p}_{-k_0} = \hat{N}_{k_0}\left(\frac{\pi}{2}, 0\right), \tag{30}$$

$$\hat{p}_{k_0} - \hat{p}_{-k_0} = \hat{N}_{k_0}\left(0, -\frac{\pi}{2}\right). \tag{31}$$

Since $\hat{q}_{k_0} + \hat{q}_{-k_0}$ and $\hat{q}_{k_0} - \hat{q}_{-k_0}$ commute, the corresponding normalized phonon operators at different times $\hat{N}_{k_0}(0,0)$ and $\hat{N}_{k_0}(\frac{\pi}{2}, \frac{\pi}{2})$ can be measured together on the same realization of the experiment. This allows one to simultaneously measure

$$\hat{q}_{k_0} = \frac{1}{2}\left[\hat{N}_{k_0}(0,0) + \hat{N}_{k_0}\left(\frac{\pi}{2}, \frac{\pi}{2}\right)\right], \tag{32}$$

$$\hat{q}_{-k_0} = \frac{1}{2}\left[\hat{N}_{k_0}(0,0) - \hat{N}_{k_0}\left(\frac{\pi}{2}, \frac{\pi}{2}\right)\right], \tag{33}$$

for each realization of the experiment. After averaging over many realizations, one can estimate the expectation values $\langle \hat{q}_{k_0} \rangle$ and $\langle \hat{q}_{-k_0} \rangle$ as well as the variances $\langle \hat{q}_{k_0}^2 \rangle$, $\langle \hat{q}_{-k_0}^2 \rangle$, and the cross product

$$\langle \hat{q}_{k_0} \hat{q}_{-k_0} \rangle = \frac{1}{4}\left[\langle \hat{N}_{k_0}(0,0)^2 \rangle - \left\langle \hat{N}_{k_0}\left(\frac{\pi}{2}, \frac{\pi}{2}\right)^2 \right\rangle\right]. \tag{34}$$

Note that, differently from a standard *in situ* measurement of the density via, e.g., phase contrast imaging [68] which simultaneously projects the many-body wave function on eigenstates of the density operators $\hat{n}(x)$ at all positions x, our proposed cavity-assisted measurement is only sensitive to the desired quadratures of the phonon operators and leaves all other quadratures and all other phonon modes unaffected. This is crucial to be able to perform a second measurement after a certain time without being disturbed by the result of the first measurement.

Analogously, the operators $\hat{p}_{k_0} + \hat{p}_{-k_0}$ and $\hat{p}_{k_0} - \hat{p}_{-k_0}$ commute, so one can measure $\hat{N}_{k_0}(\pi/2, 0)$ and $\hat{N}_{k_0}(0, -\pi/2)$ on the same realization. This allows one to construct the expectation values $\langle \hat{p}_{k_0} \rangle$ and $\langle \hat{p}_{-k_0} \rangle$ as well as all required variances $\langle \hat{p}_{k_0}^2 \rangle$, $\langle \hat{p}_{-k_0}^2 \rangle$, and cross products

$$\langle \hat{p}_{k_0} \hat{p}_{-k_0} \rangle = \frac{1}{4}\left[\left\langle \hat{N}_{k_0}\left(\frac{\pi}{2}, 0\right)^2 \right\rangle - \left\langle \hat{N}_{k_0}\left(0, -\frac{\pi}{2}\right)^2 \right\rangle\right]. \tag{35}$$

The measurement of the remaining covariance $\langle \hat{q}_{k_0} \hat{p}_{k_0} + \hat{p}_{k_0} \hat{q}_{k_0} \rangle$ requires a bit longer procedure. As the commutators

$$\begin{aligned}\left[\hat{q}_{k_0} + \hat{q}_{-k_0}, \hat{p}_{k_0} - \hat{p}_{-k_0}\right] &= \left[\hat{q}_{k_0} - \hat{q}_{-k_0}, \hat{p}_{k_0} + \hat{p}_{-k_0}\right] \\ &= \left[\hat{p}_{k_0} + \hat{q}_{-k_0}, \hat{q}_{k_0} + \hat{p}_{-k_0}\right] = 0\end{aligned} \tag{36}$$

vanish, all following quantities can be experimentally measured:

$$\begin{aligned}\left\langle \hat{N}_{k_0}(0,0) \hat{N}_{k_0}\left(0, -\frac{\pi}{2}\right) \right\rangle &= \left\langle \left(\hat{q}_{k_0} + \hat{q}_{-k_0}\right)\left(\hat{p}_{k_0} - \hat{p}_{-k_0}\right) \right\rangle \\ &= \langle \hat{q}_{k_0} \hat{p}_{k_0} \rangle - \langle \hat{q}_{-k_0} \hat{p}_{-k_0} \rangle \\ &\quad - \langle \hat{q}_{k_0} \hat{p}_{-k_0} \rangle + \langle \hat{q}_{-k_0} \hat{p}_{k_0} \rangle,\end{aligned} \tag{37}$$

$$\begin{aligned}\left\langle \hat{N}_{k_0}\left(\frac{\pi}{2}, \frac{\pi}{2}\right) \hat{N}_{k_0}\left(\frac{\pi}{2}, 0\right) \right\rangle &= \left\langle \left(\hat{q}_{k_0} - \hat{q}_{-k_0}\right)\left(\hat{p}_{k_0} + \hat{p}_{-k_0}\right) \right\rangle \\ &= \langle \hat{q}_{k_0} \hat{p}_{k_0} \rangle - \langle \hat{q}_{-k_0} \hat{p}_{-k_0} \rangle \\ &\quad + \langle \hat{q}_{k_0} \hat{p}_{-k_0} \rangle - \langle \hat{q}_{-k_0} \hat{p}_{k_0} \rangle,\end{aligned} \tag{38}$$

$$\begin{aligned}\left\langle \hat{N}_{k_0}\left(\frac{\pi}{4}, -\frac{\pi}{4}\right) \hat{N}_{k_0}\left(\frac{\pi}{4}, \frac{\pi}{4}\right) \right\rangle &= \left\langle \left(\hat{p}_{k_0} + \hat{q}_{-k_0}\right)\left(\hat{q}_{k_0} + \hat{p}_{-k_0}\right) \right\rangle \\ &= \langle \hat{p}_{k_0} \hat{q}_{k_0} \rangle + \langle \hat{q}_{-k_0} \hat{p}_{-k_0} \rangle \\ &\quad + \langle \hat{q}_{-k_0} \hat{q}_{k_0} \rangle + \langle \hat{p}_{k_0} \hat{p}_{-k_0} \rangle.\end{aligned} \tag{39}$$

Summing the first two equations, one obtains

$$\begin{aligned}\langle \hat{q}_{k_0} \hat{p}_{k_0} \rangle - \langle \hat{q}_{-k_0} \hat{p}_{-k_0} \rangle &= \frac{1}{2}\left[\left\langle \hat{N}_{k_0}(0,0) \hat{N}_{k_0}\left(0, -\frac{\pi}{2}\right) \right\rangle \right. \\ &\quad \left. + \left\langle \hat{N}_{k_0}\left(\frac{\pi}{2}, \frac{\pi}{2}\right) \hat{N}_{k_0}\left(\frac{\pi}{2}, 0\right) \right\rangle\right].\end{aligned} \tag{40}$$

Summing Eq. (40) with Eq. (39), noting that $[\hat{q}_{k_0}, \hat{q}_{-k_0}] = 0$, and using Eqs. (34) and (35), one obtains an explicit expression

for the desired cross correlation $\langle \hat{q}_{k_0}\hat{p}_{k_0} + \hat{p}_{k_0}\hat{q}_{k_0}\rangle$,

$$\begin{aligned}\left\langle \frac{\hat{q}_{k_0}\hat{p}_{k_0} + \hat{p}_{k_0}\hat{q}_{k_0}}{2}\right\rangle &= \frac{1}{2}\left\langle \hat{N}_{k_0}\left(\frac{\pi}{4},-\frac{\pi}{4}\right)\hat{N}_{k_0}\left(\frac{\pi}{4},\frac{\pi}{4}\right)\right\rangle \\ &+\frac{1}{4}\left[\left\langle \hat{N}_{k_0}(0,0)\hat{N}_{k_0}\left(0,-\frac{\pi}{2}\right)\right\rangle\right. \\ &\left.+\left\langle \hat{N}_{k_0}\left(\frac{\pi}{2},\frac{\pi}{2}\right)\hat{N}_{k_0}\left(\frac{\pi}{2},0\right)\right\rangle\right] \\ &+\frac{1}{8}\left[\left\langle \hat{N}_{k_0}\left(\frac{\pi}{2},\frac{\pi}{2}\right)^2\right\rangle\right. \\ &+\left\langle \hat{N}_{k_0}\left(0,-\frac{\pi}{2}\right)^2\right\rangle - \langle \hat{N}_{k_0}(0,0)^2\rangle \\ &\left.-\left\langle \hat{N}_{k_0}\left(\frac{\pi}{2},0\right)^2\right\rangle\right], \end{aligned} \tag{41}$$

with which the picture is complete.

Summing up, this discussion shows how a suitable series of measurements of the atomic density using an optical cavity provides full information on the whole covariance matrix V of the quadratures of a given single phonon mode in a spatially homogeneous atomic gas.

C. Spatial selectivity

This protocol is straightforwardly generalized to a spatially selective measurement of the quadratures of phonon wave-packet operators by taking into account the finite waist of the cavity mode σ_c as depicted in Fig. 7. Using the actual form (19) of the cavity mode profile, it is easy to see that the overlap now becomes a localized operator O_{k_0,x_0} proportional to a combination of spatially and spectrally localized phonon wave-packet operators of the form (3): All their correlations can then be extracted using the method described in the previous section.

The phonon quadratures at different spatial positions $x_{1,2}$ that enter the GPH function $\mathcal{P}$ can be measured by using two independent cavity modes localized at different positions $x_{1,2}$: Commutation of observables at different positions is guaranteed provided $|x_1 - x_2| \gg \sigma_c$, as shown in Sec. II. The desired wave vectors $k_{1,2}$ are selected by a suitable design of the two cavity modes. Within each cavity, the spatial shift $\Delta x_{1,2}$ is easily controlled by changing the relative phase between the two beams by, for instance, varying the optical paths from mirror 1 to mirror 2 and from mirror 3 to mirror 4, while keeping the total path constant.

Summarizing, the diagonal submatrices A and B of the covariance matrix V are extracted by applying at each position $x_{1,2}$ the method described in the previous section. The nondiagonal submatrix C is extracted by taking the average of the product of (commuting) q and p operators referring to the two regions.

V. CONCLUSIONS

In this paper we have proposed entanglement between phonon degrees of freedom as a probe to study the physics of atomic Bose-Einstein condensates. We have illustrated a viable experimental method to study the quantum coherence of the phonons emitted by analog dynamical Casimir and Hawking radiation processes. Numerical simulations show that the temperatures needed to observe entanglement are within the reach of state-of-the-art experiments and that a deep insight in the emission processes can be extracted from the rich structure of the entanglement patterns in real and momentum spaces. In particular, such an experiment would provide an unambiguous proof of the quantum origin of the analog dynamical Casimir and Hawking radiations from zero-point fluctuations.

As parametric downconversion and homodyne detection are nowadays routinely used to generate and detect entangled photons in photonics, we may anticipate that spontaneous phonon-pair generation processes and our proposed entanglement detection scheme will become standard tools to study entangled phonons in BECs.

ACKNOWLEDGMENTS

This work has been supported by ERC through the QGBE grant and by Provincia Autonoma di Trento. We are grateful to R. Balbinot, D. Gerace, R. Parentani, and J. Schmiedmayer for continuous stimulating exchanges and to C. Ciuti for providing computing resources for the numerical simulations.

[1] C. K. Hong, Z. Y. Ou, and L. Mandel, Phys. Rev. Lett. **59**, 2044 (1987).
[2] A. Aspect, Nature (London) **398**, 189 (1999).
[3] R. Raussendorf and H. J. Briegel, Phys. Rev. Lett. **86**, 5188 (2001).
[4] R. Bücker, J. Grond, S. Manz, T. Berrada, T. Betz, C. Koller, U. Hohenester, T. Schumm, A. Perrin, and J. Schmiedmayer, Nat. Phys. **7**, 608 (2011).
[5] K. V. Kheruntsyan, J.-C. Jaskula, P. Deuar, M. Bonneau, G. B. Partridge, J. Ruaudel, R. Lopes, D. Boiron, and C. I. Westbrook, Phys. Rev. Lett. **108**, 260401 (2012).
[6] M. F. Riedel, P. Böhi, Y. Li, T. W. Hänsch, A. Sinatra, and P. Treutlein, Nature (London) **464**, 1170 (2010).
[7] C. Gross, H. Strobel, E. Nicklas, T. Zibold, N. Bar-Gill, G. Kurizki, and M. K. Oberthaler, Nature (London) **480**, 219 (2011).
[8] B. Julsgaard, A. Kozhekin, and E. S. Polzik, Nature (London) **413**, 400 (2001).
[9] E. Altewischer, M. P. van Exter, and J. P. Woerdman, Nature (London) **418**, 304 (2002).
[10] S. Fasel, F. Robin, E. Moreno, D. Erni, N. Gisin, and H. Zbinden, Phys. Rev. Lett. **94**, 110501 (2005).
[11] J. Preskill, J. Mod. Opt. **47**, 127 (2000).

[12] A. Osterloh, L. Amico, G. Falci, and R. Fazio, Nature (London) **416**, 608 (2002).
[13] G. Vidal, J. I. Latorre, E. Rico, and A. Kitaev, Phys. Rev. Lett. **90**, 227902 (2003).
[14] T. J. Osborne and M. A. Nielsen, Phys. Rev. A **66**, 032110 (2002).
[15] F. Verstraete, M. Popp, and J. I. Cirac, Phys. Rev. Lett. **92**, 027901 (2004).
[16] W. Dür, L. Hartmann, M. Hein, M. Lewenstein, and H.-J. Briegel, Phys. Rev. Lett. **94**, 097203 (2005).
[17] W. G. Unruh, Phys. Rev. Lett. **46**, 1351 (1981).
[18] S. W. Hawking, Nature (London) **248**, 30 (1974).
[19] C. Barcelo, S. Liberati, and M. Visser, Living Rev. Relativ. **14**, 3 (2011).
[20] L. J. Garay, J. R. Anglin, J. I. Cirac, and P. Zoller, Phys. Rev. Lett. **85**, 4643 (2000).
[21] L. J. Garay, J. R. Anglin, J. I. Cirac, and P. Zoller, Phys. Rev. A **63**, 023611 (2001).
[22] C. Barceló, S. Liberati, and M. Visser, Phys. Rev. A **68**, 053613 (2003).
[23] P. O. Fedichev and U. R. Fischer, Phys. Rev. A **69**, 033602 (2004).
[24] M. Krämer, C. Tozzo, and F. Dalfovo, Phys. Rev. A **71**, 061602(R) (2005).
[25] P. Jain, S. Weinfurtner, M. Visser, and C. W. Gardiner, Phys. Rev. A **76**, 033616 (2007).
[26] I. Carusotto, R. Balbinot, A. Fabbri, and A. Recati, Eur. Phys. J. D **56**, 391 (2010).
[27] S. A. Fulling and P. C. W. Davies, Proc. R. Soc. London, Ser. A **348**, 393 (1976).
[28] A. Lambrecht, J. Opt. B **7**, 3 (2005).
[29] L. Parker, Phys. Rev. Lett. **21**, 562 (1968).
[30] L. H. Ford, Phys. Rev. D **35**, 2955 (1987).
[31] J.-C. Jaskula, G. B. Partridge, M. Bonneau, R. Lopes, J. Ruaudel, D. Boiron, and C. I. Westbrook, Phys. Rev. Lett. **109**, 220401 (2012).
[32] O. Lahav, A. Itah, A. Blumkin, C. Gordon, S. Rinott, A. Zayats, and J. Steinhauer, Phys. Rev. Lett. **105**, 240401 (2010).
[33] R. Balbinot, A. Fabbri, S. Fagnocchi, A. Recati, and I. Carusotto, Phys. Rev. A **78**, 021603 (2008).
[34] I. Carusotto, S. Fagnocchi, A. Recati, R. Balbinot, and A. Fabbri, New J. Phys. **10**, 103001 (2008).
[35] J. R. M. de Nova, F. Sols, and I. Zapata, Phys. Rev. A **89**, 043808 (2014).
[36] D. E. Bruschi, N. Friis, I. Fuentes, and S. Weinfurtner, New J. Phys. **15**, 113016 (2013).
[37] M. Rinaldi, Phys. Rev. D **84**, 124009 (2011).
[38] M. Rinaldi, Int. J. Mod. Phys. D **22**, 1350016 (2013).
[39] B. Horstmann, R. Schützhold, B. Reznik, S. Fagnocchi, and J. I. Cirac, New J. Phys. **13**, 045008 (2011).
[40] X. Busch, I. Carusotto, and R. Parentani, Phys. Rev. A **89**, 043819 (2014).
[41] J. Adamek, X. Busch, and R. Parentani, Phys. Rev. D **87**, 124039 (2013).
[42] X. Busch and R. Parentani, Phys. Rev. D **88**, 045023 (2013).
[43] R. Horodecki, P. Horodecki, M. Horodecki, and K. Horodecki, Rev. Mod. Phys. **81**, 865 (2009).
[44] A. Peres, Phys. Rev. Lett. **77**, 1413 (1996).
[45] P. Horodecki, Phys. Lett. A **232**, 333 (1997).
[46] L.-M. Duan, G. Giedke, J. I. Cirac, and P. Zoller, Phys. Rev. Lett. **84**, 2722 (2000).
[47] R. Simon, Phys. Rev. Lett. **84**, 2726 (2000).
[48] Y. Castin, in *Coherent Atomic Matter Waves*, edited by R. Kaiser, C. Westbrook, and F. David, Proceedings of the Les Houches Summer School of Theoretical Physics, LXXII, 1999 (Springer, Berlin, 2001).
[49] M. J. Steel, M. K. Olsen, L. I. Plimak, P. D. Drummond, S. M. Tan, M. J. Collett, D. F. Walls, and R. Graham, Phys. Rev. A **58**, 4824 (1998).
[50] A. Sinatra, C. Lobo, and Y. Castin, J. Phys. B: At. Mol. Phys. **35**, 3599 (2002).
[51] P. Calabrese and J. Cardy, Phys. Rev. Lett. **96**, 136801 (2006).
[52] A. Prain, S. Fagnocchi, and S. Liberati, Phys. Rev. D **82**, 105018 (2010).
[53] M. Gring, M. Kuhnert, T. Langen, T. Kitagawa, B. Rauer, M. Schreitl, I. Mazets, D. A. Smith, E. Demler, and J. Schmiedmayer, Science **337**, 1318 (2012).
[54] T. Kitagawa, A. Imambekov, J. Schmiedmayer, and E. Demler, New J. Phys. **13**, 073018 (2011).
[55] J. Macher and R. Parentani, Phys. Rev. A **80**, 043601 (2009).
[56] A. Recati, N. Pavloff, and I. Carusotto, Phys. Rev. A **80**, 043603 (2009).
[57] P. E. Larré, Ph.D. thesis, LPTMS, Université de Paris 11, 2013.
[58] C. M. Wilson, G. Johansson, A. Pourkabirian, M. Simoen, J. R. Johansson, T. Duty, F. Nori, and P. Delsing, Nature (London) **479**, 376 (2011).
[59] P. Lahteenmaki, G. S. Paraoanu, J. Hassel, and P. J. Hakonen, Proc. Natl. Acad. Sci. USA **110**, 4234 (2013).
[60] C. Tozzo and F. Dalfovo, Phys. Rev. A **69**, 053606 (2004).
[61] M. C. de Oliveira, Phys. Rev. A **67**, 022307 (2003).
[62] B. R. da Cunha and M. C. de Oliveira, Phys. Rev. A **75**, 063615 (2007).
[63] A. D. Cronin, J. Schmiedmayer, and D. E. Pritchard, Rev. Mod. Phys. **81**, 1051 (2009).
[64] F. Brennecke, S. Ritter, T. Donner, and T. Esslinger, Science **322**, 235 (2008).
[65] S. Ritter, F. Brennecke, K. Baumann, T. Donner, C. Guerlin, and T. Esslinger, Appl. Phys. B **95**, 213 (2009).
[66] H. Ritsch, P. Domokos, F. Brennecke, and T. Esslinger, Rev. Mod. Phys. **85**, 553 (2013).
[67] L. P. Pitaevskii and S. Stringari, *Bose Einstein Condensation* (Clarendon, Oxford, UK, 2004).
[68] M. R. Andrews, D. M. Kurn, H.-J. Miesner, D. S. Durfee, C. G. Townsend, S. Inouye, and W. Ketterle, Phys. Rev. Lett. **79**, 553 (1997).